Articles

Accommodation of an *N*-(Deoxyguanosin-8-yl)-2-acetylaminofluorene Adduct in the Active Site of Human DNA Polymerase ι: Hoogsteen or Watson−Crick Base Pairing?†

Kerry Donny-Clark,‡ Robert Shapiro,§ and Suse Broyde*,‡

Departments of Biology and Chemistry, New York University, New York, New York 10003

Received July 8, 2008; Revised Manuscript Received October 24, 2008

ABSTRACT: Bypass across DNA lesions by specialized polymerases is essential for maintenance of genomic stability. Human DNA polymerase ι (polι) is a bypass polymerase of the Y family. Crystal structures of polι suggest that Hoogsteen base pairing is employed to bypass minor groove DNA lesions, placing them on the spacious major groove side of the enzyme. Primer extension studies have shown that polι is also capable of error-free nucleotide incorporation opposite the bulky major groove adduct *N*-(deoxyguanosin-8-yl)-2-acetylaminofluorene (dG-AAF). We present molecular dynamics simulations and free energy calculations suggesting that Watson−Crick base pairing could be employed in polι for bypass of dG-AAF. In polι with Hoogsteen-paired dG-AAF the bulky AAF moiety would reside on the cramped minor groove side of the template. The Hoogsteen-capable conformation distorts the active site, disrupting interactions necessary for error-free incorporation of dC opposite the lesion. Watson−Crick pairing places the AAF rings on the spacious major groove side, similar to the position of minor groove adducts observed with Hoogsteen pairing. Watson−Crick-paired structures show a well-ordered active site, with a near reaction-ready ternary complex. Thus our results suggest that polι would utilize the same spacious region for lesion bypass of both major and minor groove adducts. Therefore, purine adducts with bulk on the minor groove side would use Hoogsteen pairing, while adducts with the bulky lesion on the major groove side would utilize Watson−Crick base pairing as indicated by our MD simulations for dG-AAF. This suggests the possibility of an expanded role for polι in lesion bypass.

Cancer initiation by bulky chemical carcinogens can stem from mutations induced by DNA adducts in oncogenes or tumor suppressors which govern cell cycle control (*1, 2*). Such bulky adducts can stall replicative polymerases, leading to a switch to lesion bypass polymerases (*3*−*5*). Human DNA polymerase ι (polι) is a lesion bypass polymerase of the Y family (Figure 1A) (*6*−*8*). Though evolutionarily related to polη (*6, 9*), polι exhibits several properties unique among DNA polymerases characterized to date. Polι has both the lowest processivity of any known DNA polymerase as well as the highest rate of misincorporation (*8, 10, 11*). The properties of polι misincorporation are also unique, in that polι exhibits differential fidelity dependent on the identity of the templating base: templating dA has the highest fidelity, with a misincorporation rate of ∼10^{-4}, while polι actually prefers to insert dG opposite dT instead of the correct partner dA (*10, 12*). This preferential misinsertion on undamaged template proved difficult to explain in structural or functional terms until the crystal structure of a polι ternary complex became available (*13*).

Crystal structures of ternary complexes of this polymerase with adenine or guanine as the templating bases reveal *syn* purines with Hoogsteen (HG) pairing (Figure 1C) in the active site (*13*−*15*). These structures suggest that HG pairing with protonated dCTP (dCTP$^+$) opposite templating guanine is favored due to specific features of the polι active site. For example, residues in the active site (Gln59, Lys60, and Leu62) grip the sugar of the templating base and induce a short C1′−C1′ distance in the nascent base pair that accommodates a narrow (∼8.7 Å) HG (dG *syn*) pair but not the wider (∼10.6 Å) Watson−Crick (WC) (dG *anti*) pairing (*15*). Related Y-family polymerases η, κ, and Dpo4, all of which employ WC pairing in the active site, have less bulky residues in the equivalent position (*16*−*18*). Crystal structures of polι ternary complexes show a preformed active site that is open and exposed to solvent on the major groove side of

† This research is supported by NIH Grant CA75449 to S.B. and R.S. and by the National Science Foundation through TeraGrid resources provided by the San Diego Supercomputer Center. Support for computational infrastructure and systems management was also provided by NIH Grant CA28038 to S.B. and R.S. The content is solely the responsibility of the authors and does not necessarily represent the official views of the National Cancer Institute or the National Institutes of Health.

* Corresponding author. Tel: (212) 998-8231. Fax: (212) 995-4015. E-mail: broyde@nyu.edu.

‡ Department of Biology, New York University.

§ Department of Chemistry, New York University.

10.1021/bi801283d CCC: $40.75
Published on Web 12/12/2008

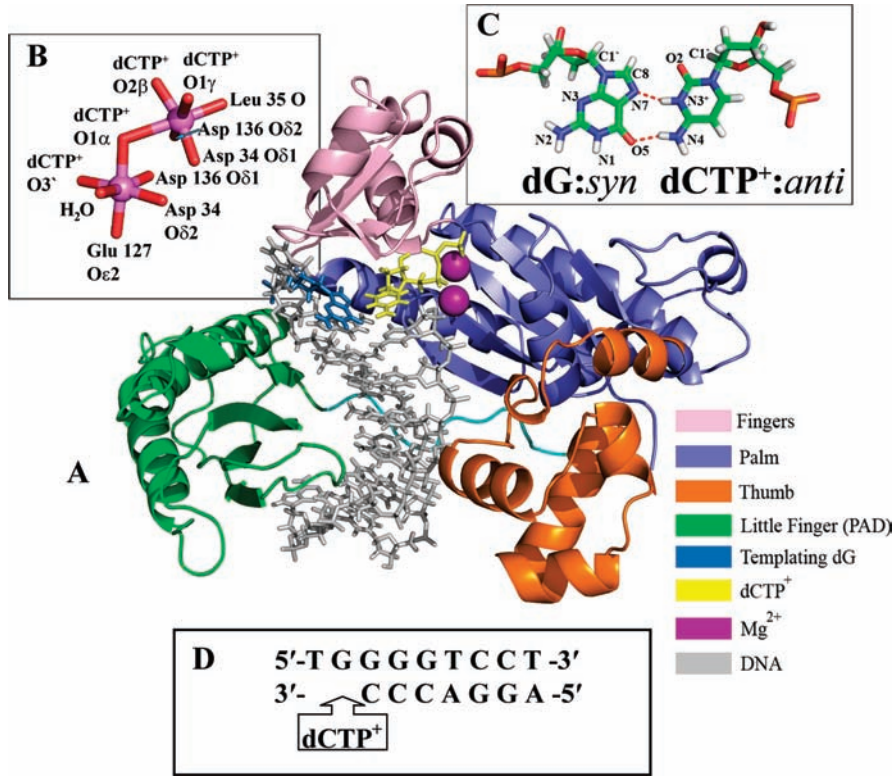

FIGURE 1: Human DNA polymerase ι with incoming dCTP$^+$. (A) Polymerase ι remodeled based on the ternary crystal structure PDB ID 2ALZ (*14*) (see Experimental Procedures for details). (B) Catalytic Mg^{2+} coordination in the initial model. Liganding distances are given in Table S8. (C) The active site Hoogsteen base pair: oxygen, red; nitrogen, blue; carbon, green; phosphorus, orange. (D) DNA sequence used in all simulations.

the nascent double helix (*13*−*15, 19*). The polymerase is close to the nascent base pair on the minor groove side, leaving little space between enzyme and the DNA. Thus, HG pairing is a novel and effective way for the polymerase to move bulky minor groove adducts away from the cramped minor groove side of the nascent base pair through rotation of the glycosidic bond to the *syn* domain. This allows for nucleotide incorporation opposite damage that compromises WC hydrogen bonding. For clarity we note that a major groove adduct would reside on the major groove side of the adducted base in normal B-DNA with WC base pairing, while a minor groove adduct would reside on the minor groove side. Numerous primer extension experiments with minor groove lesions such as N^2-dG adducts derived from benzo[*a*]pyrene diol epoxide (*20*), γ-hydroxy-1,N^2-propano-dG (*21, 22*), 3-methyladenine (*23, 24*) and N^2-methyl, -ethyl, -isobutyl, and -benzyl dG (*25*) reveal polι's capability for bypass of minor groove lesions. A ternary crystal structure of polι with the Watson−Crick edge obstructing lesion 1,N^6-ethenodeoxyadenosine (*19*) as well as biochemical data with base analogues incapable of WC hydrogen bonding (*26, 27*) also supports this hypothesis.

Polι, like other Y-family polymerases, does not use stringent steric selection or a dNTP-binding induced fit to select the incoming dNTP (*12, 15*). Furthermore, a strong case has been made for the primacy of hydrogen bonding in selecting a matching incoming nucleotide in polι (*26, 27*) and other Y-family polymerases (*12, 28, 29*). This elegantly explains the template-based differential fidelity of polι. For example, dA is able to form two hydrogen bonds with dT in both *syn* (HG) and *anti* (WC) conformations; however, if the incoming dCTP is protonated as in the polι ternary crystal structure (*14*), forming dCTP$^+$, then two HG hydrogen bonds can be formed with the templating dG *syn*. Thus polι has higher fidelity with templating dA, and lower with dG, because the A-T HG pair has two hydrogen bonds without the energetic cost of protonation that the G-C HG pair requires. When polι encounters a templating pyrimidine, the incorporation spectrum resembles that of an abasic site, which may indicate that the pyrimidine is somehow ejected from the active site (*15, 30*).

2-Acetylaminofluorene (AAF) is a mutagenic and carcinogenic aromatic amine first identified as a carcinogen during toxicity trials to determine its suitability as a pesticide (*31*). After metabolic activation, 2-acetylaminofluorene-derived carcinogens selectively react with dG to produce two major adducts, *N*-(deoxyguanosin-8-yl)-2-aminofluorene (dG-AF) and *N*-(deoxyguanosin-8-yl)-2-acetylaminofluorene (dG-AAF) (Figure 2), as well as a minor N^2-dG-AAF adduct; early work describing this field is reviewed in refs *32* and *33*. The present study focuses on dG-AAF. More recently, the dG-AAF adduct's mutagenic properties have been characterized in a wide variety of *in vitro* and *in vivo* contexts (*34*−*43*). Other investigations have focused on studies by NMR (*44*−*48*).

Primer extension studies with dG-AAF have revealed that polι predominantly incorporates dC opposite the lesion (*49*) in an error-free manner. In this experiment no extension beyond the lesion was observed, as is frequently the case in polι lesion bypass (*21, 30*). Early work at the monomer level suggested that dG-AAF favors the *syn* domain due to difficulty in avoiding steric clashes between the acetyl group on the AAF moiety and the damaged nucleotide, adopting a conformation with carcinogen-base stacking (*50*−*52*). NMR

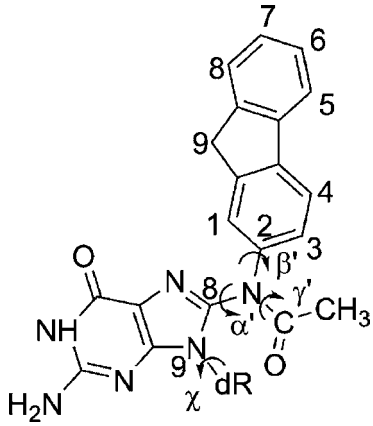

FIGURE 2: dG-AAF structure with torsion angles designated by arrows. Torsion angles at the linkage site are defined as follows: α′, N9—C8—*N*—C2; *β′*, C8—*N*—C2—C1; *γ′*, C8—*N*—C—C-(methyl); χ, glycosidic torsion angle O4′—C1′—N9—C4, where O4′, C1′, N9, C4, and C8 are from dG and other atoms are from AAF.

solution structures later showed that, as had been predicted, in double-stranded DNA dG-AAF predominantly adopts a base-displaced intercalated conformation in solution with a *syn* glycosidic torsion angle (*44, 46*), with some NMR evidence for an external conformation available as well (*53*). A base-displaced intercalated conformation displaces the templating dG, inconsistent with the error-free selection of dCTP/dCTP$^+$ opposite dG-AAF by polι. Therefore, the AAF fluorenyl rings must be placed on the major or minor groove side of the nascent base pair, with *anti* or *syn* glycosidic bond conformations, respectively. While a *syn* conformation for dG-AAF is consistent with HG pairing in polι, if the C8 adduct is *syn* (HG), the bulky AAF fluorenyl rings would be placed in a small, crowded region of the enzyme on the minor groove side of the template. With WC pairing, on the other hand, the AAF ring system would be well accommodated in the large space on the major groove side. Recently, it has been shown through MD simulations that dG-AAF can adopt the *anti* (WC) conformation with WC pairing through a modest alteration in sugar pucker in the modified nucleoside. This alleviates the steric hindrance between the acetyl and the adjacent sugar (*54*).

In the present study we investigated both WC- and HG-paired dG-AAF in polι using a molecular modeling and molecular dynamics (MD) approach supplemented by potential of mean force (PMF) analysis. Our results show that with WC pairing the AAF adduct is well accommodated on the major groove side of the growing double helix, with frequent sampling of a near reaction-ready state. HG-paired models led to severe distortion of the active site, and in no case did they sample a near reaction-ready state. In addition, free energy calculations indicate a relatively small (~5 kcal/mol) energy difference between the WC- and HG-paired dG-dCTP/dCTP$^+$ in the active site of polι. These results suggest that the dG-AAF adduct can be bypassed by polι utilizing a WC pairing scheme which places the bulky adduct on the spacious major groove side of the nascent base pair, similar to the accommodation of bulky minor groove lesions via HG base pairing in the same space. Thus polι could play a role in bypassing adducts on both the major and minor groove sides of a damaged base, adding to its versatility in human lesion bypass.

EXPERIMENTAL PROCEDURES

Molecular Modeling of Initial Unmodified Control Structures for MD. We used the polι ternary complex crystal structure containing a dG-dCTP$^+$ HG base pair (PDB (*55*) ID 2ALZ (*14*)) as the basis for our initial models. Missing loops containing residues 371−378 and residues 395−403 were modeled with the program MODELER (*56*) on the Modloop web server (*57*). The DNA sequence (Figure 1D) was taken from the crystal structure (*14*). While the crystal contained three residues in the single-stranded 5′ overhang, the last two were not resolved and are not included in our simulations. This structure was used as our HG unmodified control simulation (Figure 1A). dCTP$^+$ was modeled from dCTP by protonation of N^3. For the first Watson−Crick unmodified control simulation the glycosidic torsion angle χ (Figure 2) on the templating dG was altered from the crystal value of 64.9° (*syn*) to 254.1° (*anti*) which permitted WC pairing. A second unmodified WC structure was derived from the WC-AAF2 trajectory's most representative structure (see below). AAF atoms were deleted and replaced by a hydrogen atom, and the resulting WC unmodified structure was subjected to our molecular dynamics protocol (see below).

Molecular Modeling of Initial dG-AAF Structures for MD. Structures from the last frame (10 ns) of the unmodified control production dynamics simulations were used as the initial structures for the dG-AAF simulations (HG control for HG-AAF, WC control for WC-AAF). A high-resolution AAF structure (*58*) was obtained from the Cambridge Structural Database (*59*) (refcode ACAFLR) and bonded to C8 of the templating dG. Then the α′ and *β′* linkage torsion angles (Figure 2) of the resultant dG-AAF were surveyed over their 360° range at 10° intervals starting at 5°, with glycosidic torsion χ in the *syn* (HG) conformation (64.9°), as observed in the crystal structure (*14*) for a total of 1296 structures created. These structures were evaluated for steric clashes with the bumpcheck utility of InsightII (Accelrys Inc.). For these searches *γ′* (Figure 2) was retained in the conformation of the AAF crystal structure (*58*), i.e. 340.7°. For the *anti* WC-AAF simulations the last frame (10 ns) of the WC control structure (χ = 192.7°) was used for a similar search of an additional 1296 structures. After these initial searches were completed, α′, *β′* combinations that exhibited minimal close contacts were selected for further investigation. For the HG-AAF structures we identified two narrow regions that showed the least close contacts, one placing the fluorenyl rings 3′ of the templating dG (HG-AAF1 and HG-AAF2) and one 5′ (HG-AAF3 and HG-AAF4). For the WC-AAF structures, the AAF could be accommodated either in the broad range of α′ 260° to 284° on the exposed major groove side of the nascent base pair (WC-AAF1 and WC-AAF3) or in a narrow pocket in the little finger domain (WC-AAF2 and WC-AAF4). For both WC-AAF and HG-AAF structures each region could accommodate a pair of structures with the same α′ torsion angles, but with the methylene bridge (C9 in Figure 2) rotated ~180° about the long axis of the fluorenyl rings, which is governed by *β′*. Finally, the α′, *β′*, and *γ′* torsions of all structures were further adjusted to minimize close contacts (Figure S1, Table S1).

Force Field. The Cornell et al. force field (*60*) with modifications (*61, 62*) and the PARM99 parameter set (*63*)

were employed for all simulations. For the partial charge calculations a *syn* dG-AAF model with no steric clashes was modeled using a generic B-DNA dG from the Biopolymer module of InsightII (Accelrys Inc.) linked to a high-resolution AAF structure (*58*) from the Cambridge Structural Database (*59*) (refcode ACAFLR). The structure had C2′ *endo* envelope sugar pucker and $\chi = 34.2°$, $\alpha' = 135°$, $\beta' = 83°$, and $\gamma' = 165°$. Partial charges for the dG-AAF and for dCTP$^+$ (Tables S2 and S3) were calculated with the HF method and the 6-31G* basis set (*64*) using Gaussian 03 (*65*), and the restrained electrostatic potential fitting algorithm RESP (*66, 67*) was employed to fit the charge to each atom center. dCTP charges were taken from previous work (*68*). Parameters for atom types in dG-AAF and dCTP$^+$ not found in the PARM99 parameter set were taken from the GAFF (*69*) parameter set or developed by analogy to chemically similar atom types in the PARM99 and GAFF parameter sets. Parameters are provided in Table S4.

Molecular Dynamics Protocol. All minimizations and MD simulations used the SANDER module of the AMBER 8.0 software suite (*70*). The LEaP module of AMBER 8.0 (*70*) was used to add hydrogen atoms and neutralize the system with sufficient Na^+ atoms to bring the net charge to zero. Hydrogen atoms of the solute (DNA, polymerase, and incoming dCTP/dCTP$^+$) were minimized with implicit solvent using a distance-dependent dielectric function of $\epsilon = 4.0r$ (where r is the distance between an atom pair) for 600 steps of steepest descent, followed by 600 steps of conjugate gradient. The resulting ternary complex was reoriented with SIMULAID (*71*) to minimize the number of water molecules needed to solvate the system. A periodic TIP3P (*72*) rectangular water box with a buffer distance of 10 Å between each wall and the closest solute atom in each direction was added with the LEaP module of AMBER. Box dimensions were approximately 80 × 75 × 76 Å, with a total of ~14500 water molecules.

All systems employed the following equilibration and MD protocols: (i) minimization of the counterions and solvent molecules for 2500 steps of steepest descent and 2500 steps of conjugate gradient, with 50 kcal/mol restraints on the solute atoms; (ii) 30 ps initial MD at 10 K with 25.0 kcal/mol restraints on the solute to allow the solvent to relax; (iii) heat-up from 10 to 310 K (37 °C) at constant volume over 80 ps with 10 kcal/mol restraint on the solute; (iv) 20 ps MD at constant volume and 310 K, with 10.0 kcal/mol restraints on the solute; (v) 30, 40, and 50 ps MD at 1 atm and 310 K with decreasing restraints of 10, 1, and 0.1 kcal/mol, respectively, on solute atoms and an increasing time constant of 1.0, 2.0, and 4.0 ps, respectively, for heat bath coupling of the system; (vi) production MD was conducted at 1 atm, 310 K for 10 ns, with 1 ps coupling constants for both pressure and temperature.

In all MD simulations, long-range electrostatic interactions were treated with the particle mesh Ewald method (*73, 74*). A 9 Å cutoff was applied to the nonbonded Lennard−Jones interactions. The SHAKE algorithm (*75*) was applied to constrain all bonds involving hydrogen atoms with relative geometrical tolerance of 10^{-5} Å. The Berendsen coupling algorithm (*76*) was used for temperature scaling. A 2 fs time step was used, and the translational/rotational center-of-mass motion was removed every 0.5 ps (*77*).

Potential of Mean Force Calculations Thirty-six initial structures were generated by taking the most representative structure from the stable region of the HG control dynamics simulations (6−10 ns; see Figure S2) and resetting χ at 10° intervals from 5° to 355°. The most representative structure was identified using the trajectory clustering function in the MOIL-VIEW (*78*) program with all residues within 8.0 Å of any atom in the nascent base pair selected for analysis. Initial structures were minimized and equilibrated as described below. MD simulations were then run for 200 ps, with a 30 kcal/mol harmonic restraint centered on the initial value of χ, and χ angle values in each 200 ps ensemble were collected at 20 fs intervals. We performed three separate sets of 36 simulations with identical initial conditions and different random initial velocity distributions. All χ angle values from all three trials were used as input to a program devised by A. Grossfield to implement the weighted histogram analysis method (WHAM) (available at http://membrane.urmc.rochester.edu/) for calculating potential of mean force (relative free energy).

Stability of MD Simulations. All simulations showed reasonable stability in the active site after 4 ns and stability in the whole enzyme after ~6 ns. This was evaluated by inspecting the rmsd of the enzyme as compared to the initial state after equilibration over time (Figure S2). Therefore, all analyses presented here were performed on the final 4 ns of the trajectories.

RESULTS

In vitro primer extension data for polι containing a dG-AAF lesion as the templating base revealed that polι very strongly selects the correct partner, dC, opposite the lesion (*49*). Thus we investigated structures with incoming dCTP/dCTP$^+$ in order to determine the features that led to incorporation of the correct nucleotide opposite the adduct. We were specifically interested in whether the damaged base assumes a *syn* (HG) or *anti* (WC) conformation in the active site of the polymerase. A *syn* (HG) conformation places the bulky adduct on the cramped minor groove side of the growing double helix, while an *anti* (WC) conformation places the AAF lesion on the spacious major groove side. We performed 11 molecular dynamics simulations: three unmodified controls, one with undamaged *syn* (HG) and two with undamaged *anti* (WC) dG as the template, and eight dG-AAF damaged template simulations: four *syn* (HG) and four *anti* (WC). Initial α' and β' torsion angles (Figure 2, Table S1, Figure S1) for the adduct were selected through an extensive conformational search of 2592 structures as detailed in the Experimental Procedures. We performed 10 ns of production MD for each structure, with the final 4 ns used for analysis.

Criteria for a Near Reaction-Ready State. Using the well-organized active site of a high-resolution polβ crystal structure containing two Mg^{2+} ions and a primer terminal 3′ OH (*79*) and the results of a quantum mechanical molecular modeling study (*80*) as our guides, we utilize the following structural criteria for a near reaction-ready state: (1) a Pα−O3′ distance of less than 3.5 Å, (2) an O3′−Pα−O3α angle of attack of 170 ± 10°, and (3) reasonable coordination of the two catalytic Mg^{2+} ions (Figure 1B) (discussed below). Furthermore, as a reasonably stringent criterion for a near

Table 1: Near Reaction-Ready Occupancy and Number of Hydrogen Bonds Formed between the Incoming dCTP(WC)/dCTP$^+$(HG) and the Templating dG (Control)/dG-AAF (Damaged)

structures	HG control	WC control 1	WC control 2	HG-AAF1	HG-AAF2	HG-AAF3	HG-AAF4	WC-AAF1	WC-AAF2	WC-AAF3	WC-AAF4
near reaction-ready occupancy (%)	51	82	83	0	0	0	0	76	75	0.4	70
no. of hydrogen bonds	2	3	3	0	0	0	1	2	3	3	3

reaction-ready active site we evaluated the percentage of structures in our trajectories that satisfy all three of the above criteria simultaneously and term that the near reaction-ready occupancy (Table 1).

We also considered the extent of hydrogen bonding between the incoming dCTP/dCTP$^+$ and the templating base in order to determine if proper HG or WC hydrogen bonding was taking place (Table S5). In addition, we analyzed hydrogen bonding between the nascent base pair and the enzyme, using the unmodified control HG simulation as our benchmark (Tables S6 and S7). Our criteria for hydrogen bonding are a donor and acceptor heavy atom distance of <3.4 Å and a donor−hydrogen−acceptor angle of $180° \pm 55°$. Finally, we have used WHAM (*81*) to derive the free energy profile around the glycosidic bond for the HG unmodified control simulation to gain energetic insight into the overall cost of forming an *anti* structure in the active site.

WC and HG Unmodified Control Simulations Share Some Common Features in the Active Site. Both HG and WC unmodified control simulations were performed and analyzed as described above. The most representative active site structure was identified using the trajectory clustering function in the MOIL-VIEW (*78*) program with all residues within 8.0 Å of any atom of the nascent base pair selected for analysis. The fingers domain of the enzyme shows the highest degree of stability, with a fingers domain backbone rmsd of <1 Å between the most representative active site structure of any of the unmodified control simulations and the crystal structure. All of the active site hydrogen bonds between the incoming nucleotide and the enzyme observed in the crystal are maintained in the HG and both WC unmodified control simulations, with the exception of the hydrogen bond between Tyr68 and the incoming dCTP/dCTP$^+$, which is replaced by two hydrogen bonds with water in all three simulations (Table S6). In other respects the unmodified control simulations differ, as described below.

Hoogsteen Unmodified Control Is Faithful to the Crystal Structure. All ternary complex crystal structures of polι to date show a HG pair formed between the incoming dNTP and the templating base (*13*−*15, 19*). In our unmodified control simulation the *syn* (HG) conformation of the templating base is maintained throughout the HG unmodified control simulation (Figure S3). The structural features of the active site are similar to the crystal, with a HG compatible C1′−C1′ distance of 8.8 ± 0.2 Å (Figure S4). Good base stacking is observed between the incoming dCTP$^+$ and the primer terminus (Figure S5). The Mg^{2+} ions are well coordinated (discussed below) (Figures S6 and S7, Table S8), though the inter-Mg^{2+} distance does increase somewhat, from 3.4 to 4.1 ± 0.1 Å. Overall near reaction-ready occupancy for the HG unmodified control is 51% (Table 1), a figure that is not surprising given polι's extremely slow rate of incorporation (*8, 10*). Hydrogen bonding in the nascent base pair is good, with both HG hydrogen bonds present at $>99\%$ occupancy (Table 1, Table S5). Other features of the active site resemble the ternary crystal structure (*14*), with the close C1′−C1′ distance enforced by the tight coordination of the incoming dCTP$^+$ via numerous hydrogen bonds (Table S6) and other polar interactions coupled with the stabilization of the templating base's sugar by Gln59, Lys60, and Leu62 (Figure 3A). Lys60 forms a hydrogen bond with the free phosphates in the templating dG backbone, contributing to the HG-compatible C1′−C1′ distance (Figure 3A, Table S7). Ser307, on the other hand, forms a hydrogen bond with the dT 5′ overhang phosphate group, as opposed to hydrogen bonding with the dG backbone phosphate as in the crystal structure, due to a shift in the position of the mobile little finger domain (*12*). This change in hydrogen bonding does not appear to impact the organization of the nascent base pair or the active site as a whole.

Watson−*Crick Unmodified Control Loses Important Contacts with the Polymerase.* In order to evaluate the feasibility of accommodating a WC pair in the active site of polι, we performed two simulations: (1) WC unmodified simulation 1, where the initial structure was identical to the HG unmodified control, except that the templating base was initiated with an *anti* (WC) conformation (Table S1), and (2) WC unmodified simulation 2, a WC unmodified simulation using the most representative structure from the WC-AAF2 simulation, with the AAF moiety replaced by a hydrogen atom, as the initial state; WC-AAF2 showed the highest reaction-ready occupancy of the WC-AAF simulations. This simulation was suggested by a reviewer.

In both simulations the incoming dCTP was unprotonated so as to allow three WC hydrogen bonds to form. These simulations performed surprisingly well, both attaining a standard WC C1′−C1′ distance of 10.6 ± 0.2 Å (*82*) which was then maintained throughout the stable region of the trajectory (Figure S4). For both simulations base stacking between the nascent pair and the previously incorporated pair is not disrupted (Figure 3C, Figure S5). Mg^{2+} coordination does not differ significantly from the HG unmodified control in either case (Figures S6 and S7, Table S8), and the inter-Mg^{2+} distance is 3.9 ± 0.1 Å in both simulations. Both simulations have two Watson−Crick hydrogen bonds that are present at $>99\%$ occupancy, with the third at $\sim 86\%$ occupancy in WC unmodified 1 and $\sim 98\%$ in WC unmodified 2 (Table S5). In addition, a hydrogen bond between Gln59 and N^2 of the templating dG is formed in both simulations, with $\sim 98\%$ occupancy in WC unmodified 1 and $\sim 77\%$ occupancy in WC unmodified 2 (Table S7). This hydrogen bond is not possible with the *syn* template in the HG pair. Moreover, the near reaction-ready occupancy is 82% for WC unmodified 1 and 83% for WC unmodified 2 (Table 1).

We sought to define the structural rearrangements associated with forming such a near reaction-ready Watson−Crick

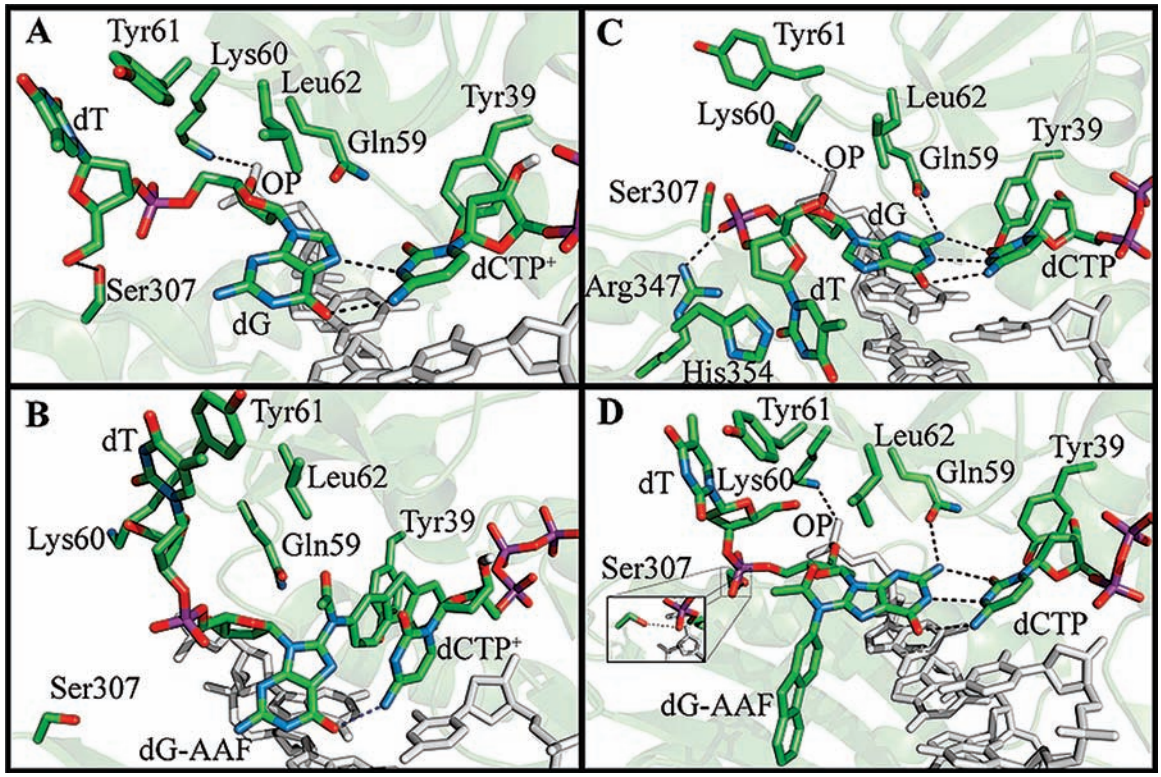

FIGURE 3: Active site organization and hydrogen bonds formed by the templating dG/dG-AAF. Pol*ι* is in green, duplex DNA is in gray, and key active site features are colored by atom: oxygen, red; nitrogen, blue; carbon, green; phosphorus, purple. Stereoviews are available in Supporting Information, Figure S11. (**A**) Unmodified HG control simulation. Two HG hydrogen bonds are formed between the incoming $dCTP^+$ and the template. Hydrogen bonds between Ser307 and the terminal dT O5′ and between Lys60 and a backbone oxygen from the previously incorporated dG (labeled as OP) stabilize the base position. Note the stacking of the dT single-stranded overhang with Tyr61. (**B**) HG-AAF4. This structure was selected as the least distorted HG-AAF structure (Table 1). Note the absence of hydrogen bonding between the templating dG-AAF and the enzyme and the single hydrogen bond between dG-AAF and $dCTP^+$. (**C**) Unmodified WC control simulation. Three WC hydrogen bonds are formed between dG and dCTP. The hydrogen bond between Ser307 and the terminal O5′ is replaced by a hydrogen bond between Arg347 and a backbone oxygen from the templating dG, and the 5′ dT overhang stacks with His354 instead of Tyr61. Lys60 forms a hydrogen bond with a backbone oxygen from the previously incorporated dG (labeled as OP) as in the HG control. The dG sugar ring is pulled away from residues Gln59, Lys60, and Leu62. A novel hydrogen bond not possible in the HG conformation is formed between Gln59 and N^2 of the templating dG. (**D**) WC-AAF2. The active site is stabilized by hydrogen bonds from a templating dG backbone oxygen to Lys60 and from a backbone oxygen on the previously incorporated dG (labeled OP) to Ser307, as well as the novel hydrogen bond between Gln59 and N^2 of the templating dG observed in the WC control. Three WC hydrogen bonds are formed in the nascent base pair, and the 5′ dT overhang stacks with Tyr61 as in the HG control.

pair in the unmodified control simulations. In both cases the hydrogen bonds between the incoming dCTP and the polymerase are similar to the HG unmodified control (Table S6). However, in order to stabilize a wider C1′−C1′ distance, the dT 5′ to the templating dG moves toward the major groove side of the nascent base pair, pulling the DNA backbone away from the polymerase. In WC unmodified control 1 the single-stranded overhang stacks with a histidine (His354) in the little finger domain, pulling the C1′ carbon of the templating dG ~2 Å away from the active site (Figure 3C). In WC unmodified control 2 the 5′ OH of the overhang hydrogen bonds with N^7 of the templating dG. Since the incoming dCTP remains stably positioned relative to the fingers domain of the protein in both cases, the movement of the overhang and backbone away from the confines of the polymerase allows the C1′−C1′ distance to increase to ~10.6 Å, appropriate for a WC pair (*82*) (Figure S4), and the sugar pucker is a B-DNA standard C2′ *endo* (*82*) (Table S9). In both cases the DNA template backbone also loses the hydrogen bond with Ser307 found in the HG unmodified control simulation due to the rearrangement of the backbone. This hydrogen bond is replaced with a hydrogen bond to Arg347 in the little finger domain in WC control 1 but is lost entirely in WC control 2 (Figure 3C, Table S7). This major groove position of the single-stranded base 5′ to the template is not seen in any of the other simulations, and neither of these structures would be feasible if the 5′ overhang were longer (Figure 3C) due to a dearth of room on the major groove side of the duplex. This implies that such a WC permissive conformation in the enzyme with unmodified DNA is likely to be disfavored during replication, consistent with the crystallographic observations to date.

Hoogsteen AAF Simulations Show a Variety of Distortions That Prevent Achievement of a Near Reaction-Ready State. Of the 1296 initial models of dG-AAF with HG pairing that we screened (see Experimental Procedures and Supporting Information) we selected four with minimal close contacts between the adduct and the enzyme for further study. HG-AAF MD simulations differed in the combined initial values of the torsion angles α′, *β*′, and *γ*′ and, therefore, the placement of the lesion relative to the DNA and polymerase (Figure S1, Table S1). Two initial structures placed the AAF rings 3′ to the templating dG (HG-AAF1 and HG-AAF2), and two placed the AAF rings 5′ to the templating dG (HG-AAF3 and HG-AAF4) (Figure S1). Both members of each pair of structures place the fluorenyl rings in the same region

relative to dG, but the methylene bridge (C9 in Figure 2) is rotated ~180° around the long axis of the fluorenyl rings in the pair members (Figure S1). After 10 ns of simulation the active site is severely distorted in all four cases, with no common motifs for placement of the AAF (Figure 3B, Figures S8 and S9). Hydrogen bonding between the incoming $dCTP^+$ and templating dG-AAF is poor or absent (Table 1, Table S5), Pα−O3′ distances are long (Figure S4), and base stacking between the incoming $dCTP^+$ and the primer terminus is often disrupted (Figure S5). While hydrogen bonds between the incoming $dCTP^+$ and the enzyme are mostly maintained (Table S6), the interactions between the templating base and the enzyme are lost or altered in the majority of the HG dG-AAF simulations (Figure 3B, Table S7). Most importantly, the HG dG-AAF structures, without exception, have a near reaction-ready occupancy of 0% (Table 1), strongly suggesting that incorporation of the incoming $dCTP^+$ would be disfavored.

The HG dG-AAF structures attempt to accommodate the lesion in different ways. The bulky hydrophobic fluorenyl moiety stacks with the cytosine ring of the incoming $dCTP^+$ in the HG-AAF1, HG-AAF2, and HG-AAF4 simulations (Figures S8 and S9). In the HG-AAF2 and HG-AAF4 cases this causes the cytosine ring to rotate ~90° around the glycosidic bond, disrupting hydrogen bonding with the dG-AAF (Figure 3B). Accommodation of the lesion has the additional effect of displacing the modified guanine from the double helix in all trials save HG-AAF3 (Figures S8 and S9), resulting in increased C1′−C1′ distances (Figure S4). The primer terminus disengages from the active site, in the case of HG-AAF2 moving as far as 11 Å away from the incoming $dCTP^+$ Pα (Figure S4). The acetyl moiety of dG-AAF is placed 3′ to the dG-AAF when there is significant displacement of the base and otherwise is placed 5′ of the guanine rings (Figures S8 and S9).

Watson−Crick AAF Simulations Accommodate the Lesion Well with Little Distortion of the Active Site. When dG-AAF was modeled with an *anti* (WC) glycosidic torsion angle, four structures were again selected as initial models for MD simulation from a scan of 1296 possible conformations (see Experimental Procedures and Supporting Information) (Table S1, Figure S1). In all four cases the active site is stable and well ordered after MD simulation (Figure 3D, Figures S8 and S9). As seen in Table 1, there are three hydrogen bonds between the templating base and dCTP in all simulations; their occupancies range from 59% to 100% (Table S5). Base stacking between the incoming dCTP and the primer terminus is well maintained (Figure S5), and the C1′−C1′ distance is near the typical WC value of 10.6 Å (Figure S4). The WC-AAF1, WC-AAF2, and WC-AAF3 simulations produce near reaction-ready occupancies (involving good Pα−O3′ distance (Figure S4), Mg^{2+} coordination (Figures S6 and S7, Table S8), and in-line attack angle (Figure S3, Table S9) of >70%. However, the WC-AAF3 simulation showed only 0.4% occupancy (Table 1) due to an overlong Pα−O3′ distance (Figure S4) resulting from a hydrogen bond between Tyr39 and O3′ of dCTP (Figure S10, Table S6). This hydrogen bond pulls the dCTP Pα away from O3′ of the primer terminus, and it is not observed in other WC-AAF simulations (Table S6).

The dG-AAF does not significantly disrupt the active site in these simulations. Analysis of the four trials reveals two motifs for placement of the fluorenyl rings and acetyl group of the dG-AAF. WC-AAF1 and WC-AAF3 simulations had the fluorenyl rings placed 5′ to the damaged base, thus stacking with the 5′ overhang dT (Figure S8). The acetyl moiety is 3′ to the guanine rings, causing a change in the sugar pucker to the C1′ *exo* domain in order to avoid close contacts with the acetyl (Figures S3 and S8, Table S9). The remaining two simulations have the fluorenyl rings 3′ to the dG, allowing the 5′ overhang to stack with Tyr61. The acetyl is 5′ to the base, and the sugar is C1′ *exo* (WCAAF2) or O4′ *endo* (WCAAF4) (Figures S3 and S8, Table S9). The alteration of the sugar pucker is consistent with previous results in Dpo4, which also showed that a C1′ *exo* pucker permitted *anti* dG-AAF (*54*). Hydrogen bonding between the incoming dCTP and polι is robust, with no significant differences from the HG unmodified control (Table S6).

In these simulations the increased C1′−C1′ distance necessary for WC pairing was made possible by an adjustment of the sugar on the templating base that moves the C1′ carbon away from the incoming dCTP. Unlike the WC unmodified control there is no stacking between the template 5′ dT overhang and the little finger domain. The templating dG-AAF forms strong hydrogen bonds with Gln59 and Lys60 (Figure 3D, Table S7), helping to maintain contact with the hydrophobic residues that hold the dG-AAF sugar. The fingers domain adjusts slightly to accommodate the new placement of the sugar on the templating base, with the residues in the vicinity of the sugar (i.e., Gln 59 to Leu62) moving ~1 Å relative to the rest of the fingers domain. The remainder of the active site protein backbone is relatively static, with an average rmsd of 0.50 Å between the WC dG-AAF structures and the crystal structure.

Mg^{2+} Coordination in Our Simulations Is Less Than Ideal. The two catalytic Mg^{2+} ions in the polι active site are each coordinated by six electronegative oxygen atoms (Figure 1B). We consider good Mg^{2+} coordination in polι as one Mg^{2+} ion with all six oxygens within 2.4 Å and the other Mg^{2+} with five of these oxygens within 2.4 Å and one oxygen within 3.2 Å (see Discussion). In the simulations which exhibit good Mg^{2+} coordination, all but one of the coordinating oxygens are within 2.4 Å. The exception is the only O that is involved in coordinating both Mg^{2+} ions, dCTP/$dCTP^+$ O1α. The O1α is within 2.4 Å of either $Mg^{2+}{}_A$ or $Mg^{2+}{}_B$, but never both at the same time. Time course analyses and Mg^{2+} coordination mean distance and standard deviation values for the stable region of the dynamics are shown in Figures S6 and S7 and Table S8.

Free Energy Analysis with Incoming $dCTP^+$ Shows both Syn and Anti Conformations Occupy Energy Wells, with Syn Lower in Energy. In light of our findings above indicating that a WC pair can be stably accommodated in the active site of polι we sought to estimate the overall energetic cost of maintaining an *anti* conformation of the templating base relative to a *syn* conformation. We used the weighted histogram analysis method (WHAM) (*81*) on a series of umbrella samples (see Experimental Procedures) which scanned over the entire range of the glycosidic torsion angle χ. Analysis of the relative free energy around χ for the most representative HG unmodified control structure with incoming $dCTP^+$ showed that the *syn* structure is ~5 kcal/mol lower in energy than the *anti* structure (Figure 4A). Both of

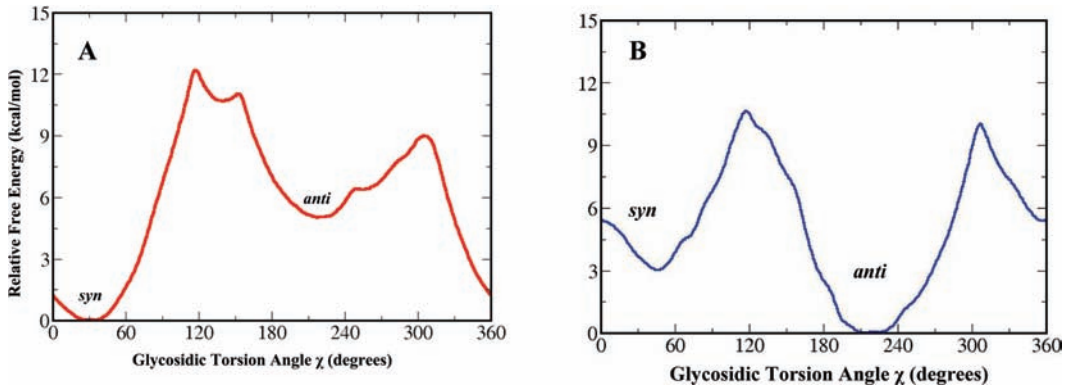

FIGURE 4: (A) Free energy profile for rotation around the glycosidic torsion angle χ in the Hoogsteen control structure with incoming dCTP$^+$. Minima correspond to the *syn* (33°) and *anti* (217°) domains, with *syn* ~5 kcal/mol lower in energy. (B) Free energy profile for rotation around the glycosidic torsion angle χ in the Hoogsteen control structure with incoming unprotonated dCTP. Minima correspond to the *syn* (43°) and *anti* (211°) domains, with *anti* ~3.5 kcal/mol lower in energy.

the *syn* and *anti* structures lie in energy wells, and they are separated by barriers of ~12 and ~9 kcal/mol, depending on the direction of the rotation. While this simulation was performed with a protonated dCTP$^+$, which precludes formation of three WC hydrogen bonds, nevertheless the *anti* structure resides in an energy well. When the proton is removed from the dCTP, the difference is ~3.5 kcal/mol, but the *anti* structure has the lower energy, and the barriers are both ~10 kcal/mol (Figure 4B). The presence of an *anti* energy well separated from the *syn* domain well by an ~9−10 kcal/mol barrier regardless of the protonation state of the incoming nucleotide would preclude the interconversion of *anti* (WC) and *syn* (HG) structures within the time frame of our simulations.

DISCUSSION

The discovery that polι utilizes HG pairing in the active site to select the newly incorporated nucleotide showed that DNA polymerases can be more versatile than was previously believed. In light of previous work on accurate dG-AAF bypass by polι (*49*) we investigated how polι incorporated a correct partner opposite dG-AAF. Preliminary modeling showed that a *syn* conformation of the dG-AAF would place the bulky AAF fluorenyl rings on the cramped minor groove side in close contact with the enzyme, while an *anti* conformation was free of steric hindrance. Accordingly, we hypothesized that WC base pairing was necessary for selection and incorporation of dCTP opposite dG-AAF. A series of MD simulations based on an extensive search for optimal initial structures strongly supported this hypothesis.

Rationale for a WC Conformation of dG-AAF in Polι. Polι is unique in many ways. It is the least accurate, least processive polymerase discovered to date (*8, 10, 11*). In addition, it is the only polymerase observed to use a HG-paired *syn* templating base in the active site with both undamaged and damaged DNA (*13*−*15, 19*). However, our results show WC base pairing with dG-AAF in the active site (Figure 3, Figures S8 and S9). In this case WC pairing is consistent with the mechanism of damage bypass proposed for polι based on its crystal structures.

Polι has been shown to enable nucleotide incorporation opposite minor groove lesions or lesions that compromise WC hydrogen bonding via a HG pair (*19*−*25*); this places the damage away from the cramped minor groove side of the protein and into the spacious major groove side. Our results show that AAF, a bulky major groove lesion, is also readily placed into the same spacious major groove region in order to facilitate nucleotide incorporation opposite the damaged base (Figure 3D, Figures S8 and S9).

In addition, the series of binary and ternary crystal structures of polι (*13*−*15*) show that the templating base is in the *anti* conformation in the binary complex. The incoming nucleotide forces the templating base to rotate ~180° around the glycosidic bond, in order to form a HG pair in the ternary complex. The energetic cost of this rotation is therefore less than the cost of adjusting the protein to accommodate the increased C1′−C1′ distance required for WC pairing. However, if there were a large, bulky major groove lesion on the templating base, such as AAF, the cost of the rotation would increase greatly. This alters the energy landscape and would plausibly make remaining in the *anti* conformation more energetically favorable than rotating to *syn*. The results observed by Choi and Guengerich with increasingly bulky adducts linked to N^2 of guanine (*25*) may stem from a similar effect. Though polι can incorporate dCTP opposite these lesions, the efficiency of incorporation decreases with increasing size of the lesion, with strong effects seen even for N^2-methyl-dG. This is hard to explain, as the *syn* conformation would place these adducts on the major groove side of the enzyme, which is spacious enough to accommodate adducts as large as AAF. However, the energetic cost of rotating the damaged dG through an area occupied by either the protein or the nascent DNA duplex would increase with the bulk of the damage. This could account for the observed decrease in efficiency for increasingly bulky dG N^2 adducts, which could block incorporation if they remained on the cramped minor groove side.

Structural Features of AAF and Unmodified Control Simulations Suggest That WC Pairing Is Preferred for Incorporation Opposite dG-AAF but Not Undamaged dG. Our simulations for the unmodified control WC systems suggest that this pairing scheme is unlikely without the dG-AAF lesion. Our first unmodified control Watson−Crick structure was facilitated by a stacking interaction between His354 and the 5′ dT overhang on the templating strand that stabilized a WC compatible C1′−C1′ distance (Figure 3C). This 5′ overhang stacking appears to be infeasible with a longer single-stranded template region, as would be found

in a replicative context. A second simulation with an unmodified WC pair derived from a WC dG-AAF simulation showed similar structural rearrangements, further supporting the idea that WC pairing is only possible with conformations placing the 5′ single-stranded overhang on the major groove side of the templating base, away from the polymerase. The widened C1′−C1′ distance needed for WC pairing is stabilized by this abnormal position of the overhang. In polι the force on the nascent WC base pair due to the long C1′−C1′ distance is alleviated by a reorientation of the template backbone and the movement of the 5′ dT overhang to the major groove side. Addition of another base or bases on the 5′ side of the templating dG would not much alter this; however, if the single-stranded overhang were very long, as in a replicative situation, this force would have to be alleviated in a different way, such as by rotating to a *syn* conformation.

Biochemical experiments with 7-deazaguanine as the templating base support the likelihood of Hoogsteen pairing in the unmodified case (*26*). Though the 7-deazaguanine is capable of WC pairing, one hydrogen bond of the HG pair is disrupted. Since nucleotide incorporation opposite the 7-deazaguanine by polι is severely impaired, a strong dependence upon HG pairing is suggested.

Since the crystal structure (*14*) reveals a protonated *syn* dCTP$^+$, the protonated state is clearly favored energetically for the *syn* conformation; the added hydrogen bond contributes to the energy needed for protonation, which likely occurs in the *syn* domain just as proper alignment for HG base pairing is achieved. The *anti* conformation, however, would disfavor protonation, since no structural advantage arises. Experimental investigations of the pK_a of N^3 protonated cytosine in triple helices containing HG base pairs (*83*−*85*) indicate that the N^3 pK_a is ∼3−5 units above that of free cytosine (∼4.3) (*86*). This corresponds to a stabilization energy range of ∼4−7 kcal/mol for the N^3 in HG-paired cytosine, with the higher value appearing more probable according to the pK_a data (*83, 84*). Clearly, many factors (*83*−*85*) govern this value. Our energy analyses by umbrella sampling over the glycosidic torsion angle χ for dCTP$^+$ and dCTP (Figure 4) were notable in indicating energy wells for the *anti* conformation in both cases. With the pK_a data and the concept that the protonation and the pK_a change occur just in time to facilitate HG pairing in the *syn* conformation one could propose that the *syn* well in Figure 4B is lowered by ∼4−7 kcal/mol by protonation. This would give an energy difference between *syn* dG-dCTP$^+$ and *anti* dG-dCTP ranging between 0.5 and 3.5 kcal/mol, in favor of *syn* dG-dCTP$^+$, with the higher value being more likely. Thus the WC conformation is unlikely to occur in the unmodified case, consistent with the ternary crystal structures and biochemical data (*13*−*15, 19, 26, 27*).

However, our simulations suggest that with the presence of the AAF lesion WC pairing becomes favorable. In the WC dG-AAF simulations WC pairing accommodates the bulky AAF moiety on the spacious major groove side of the enzyme. The high near reaction-ready occupancies we observed for the WC-AAF simulations suggest that these structures are plausible (Table 1).

Examination of the MD ensembles for the WC-AAF simulations sheds some light on the changes necessary in the enzyme in order to accommodate a WC dG-AAF/dCTP pair in the active site. In their series of crystallographic studies of polι Nair et al. (*13*−*15, 19*) note the importance of three amino acids in the fingers domain (Gln59, Lys60, and Leu62) that hold the sugar of the templating base in a small hydrophobic cavity, leading to a short C1′−C1′ distance. This in turn forces the templating base to assume a *syn* conformation to avoid clashing with the incoming nucleotide. In the unmodified WC control structures the sugar of dG loses van der Waals contacts with these three residues, allowing an increase in the C1′−C1′ distance (Figure 3C). However, in the WC-AAF simulations the sugar remains in the cavity, and the increased C1′−C1′ distance is enabled by a slight conformational change in the fingers domain of residues Gln59, Lys60, and Leu62 (Figure 3D). Residues Gln59, Lys60, and Leu62 move ∼2 Å relative to the remainder of the fingers domain and the active site in order to accommodate a wider C1′−C1′ distance in the WC-AAF simulations. The active site is otherwise essentially unchanged. Thus, in the case of a damaged dG-AAF template, WC pairing is allowed without sacrificing other important contacts between the nascent base pair and the active site. Two additional hydrogen bonds in the active site may help to compensate for the energetic cost of rearranging the enzyme to allow a wider C1′−C1′ distance: one additional hydrogen bond in the nascent base pair and a hydrogen bond between the *anti* templating dG and Gln59, not possible in the *syn* conformation (Figure 3C,D). The unmodified WC controls, while also manifesting these hydrogen bonds, assume a conformation unlikely in a replicative context and loses significant DNA/protein contacts (Figure 3C).

HG-Paired dG-AAF Structures Appear Unlikely To Lead to Nucleotide Incorporation Due to Numerous Active Site Distortions. In contrast to the well-ordered active sites observed in the WC-AAF simulations the HG-AAF simulations show a disparate collection of distortions, all of which would impede incorporation of dCTP$^+$ opposite the lesion (Figure 3B, Figures S8 and S9). As a result all of the HG-AAF structures have a near reaction-ready occupancy of 0% (Table 1). These distortions include loss of Mg^{2+} coordination, loss of hydrogen bonding between incoming dCTP$^+$ and template as compared to the unmodified control HG simulation, dramatically increased Pα−O3′ distances, and displacement of the incoming nucleotide away from the template (Figure 3B, Figures S8 and S9, Tables S6 and S8). None of the four initial simulations yielded a near reaction-ready structure, indicating that the observed incorporation of dCTP/dCTP$^+$ opposite dG-AAF (*49*) would not likely result from an HG pair. Just as polι uses a *syn* conformation for the template to put bulky minor groove adducts on the spacious major groove side, our results suggest that it can use an *anti* conformation to place bulky major groove adducts such as dG-AAF on the major groove side as well.

Coordination of Mg^{2+} Ions in Polι Is Imperfect. All of our simulations, both with damaged and undamaged DNA, show somewhat impaired Mg^{2+} coordination of either the catalytic Mg^{2+} ion, $Mg_A{}^{2+}$, or the nucleotide binding Mg^{2+} ion, $Mg_B{}^{2+}$ (Figures S6 and S7, Table S8). In addition, recent results show that polι has higher fidelity and processivity with Mn^{2+} (*24, 87*), which has a looser coordination requirement than Mg^{2+}, as the catalytic ion. Together, these results may indicate that the polι active site does not favor ideal coordination of the catalytic Mg^{2+} ions. This is

consistent with polι's slow rate of nucleotide incorporation with Mg^{2+} ions (*8, 10*). Our simulations support this insofar as no simulation showed perfect octahedral coordination of both Mg^{2+} ions simultaneously at any time. However, current force field issues concerning proper treatment of Mg^{2+} ions are still a frontier issue (*88*). In this connection, simulations of large systems such as in the present work are necessarily subject to current approximations in the state of the art including force field and sampling considerations (*89*).

CONCLUSION

Our results elucidate how human DNA polymerase ι is able to incorporate a correct partner opposite a major groove lesion. Primer extension results show that polι is capable of nucleotide incorporation opposite structurally diverse lesions, including a variety of minor groove adducts (*20*−*22, 25*) and major groove adducts (*90*), as well as thymine and uracil dimers (*30, 91, 92*) and abasic sites (*10, 49, 93*). Our results lend insight into this process, explaining in structural terms how polι correctly incorporates dCTP opposite a major groove dG-AAF lesion. Though polι's function *in vivo* has been difficult to discern, recent results indicating that polι may be responsible for the dramatically increased cancer rate of XPV patients (*94*), who lack functional polη, show that understanding polι on a structural level may relate to human health. If polι must substitute for polη in XPV patients, it may be called upon to contribute to bypass of a variety of lesions, both major and minor groove, in cells that have lost the function of other, more reliable bypass polymerases. In conclusion, our study suggests an expanded role for polι in lesion bypass that could include both major and minor groove adducts, utilizing both WC and HG base pairing to place bulky lesions on the spacious major groove side.

ACKNOWLEDGMENT

We thank Dr. Lei Jia for careful reading of the manuscript and helpful suggestions. We also wish to acknowledge excellent suggestions provided by one of the reviewers. Figures were created with Pymol (DeLano Scientific LLC) and Matlab (The Mathworks, Inc).

SUPPORTING INFORMATION AVAILABLE

Figures: S1, initial dG-AAF conformations; S2, rmsd vs time plot; S3, torsion angles vs time plot; S4, C1′−C1′ and Pα−O3′ distances vs time plot; S5, base stacking; S6 and S7, Mg^{2+} coordination distances vs time plots; S8, most representative structure active site stereoviews; S9, most representative structure whole enzyme stereoviews; S10, WC-AAF3 active site with hydrogen bonds; S11, stereoviews of the active site structures shown in Figure 3. Tables: S1, initial torsions for all structures; S2−S4, AMBER parameters; S5−S7, hydrogen bond occupancies; S8, average Mg^{2+} coordination distances; S9, torsion angle ensemble average values. This material is available free of charge via the Internet at http://pubs.acs.org.

REFERENCES

1. Luch, A. (2005) Nature and nurture—lessons from chemical carcinogenesis. *Nat. Rev. 5*, 113–125.
2. Clapp, R. W., Jacobs, M. M., and Loechler, E. L. (2008) Environmental and occupational causes of cancer: New evidence 2005–2007. *Rev. Environ. Health 23,* 1–37.
3. Friedberg, E. C., Lehmann, A. R., and Fuchs, R. P. (2005) Trading places: how do DNA polymerases switch during translesion DNA synthesis? *Mol. Cell 18*, 499–505.
4. Lehmann, A. R. (2006) Translesion synthesis in mammalian cells. *Exp. Cell Res. 312*, 2673–2676.
5. Lehmann, A. R., Niimi, A., Ogi, T., Brown, S., Sabbioneda, S., Wing, J. F., Kannouche, P. L., and Green, C. M. (2007) Translesion synthesis: Y-family polymerases and the polymerase switch. *DNA Repair (Amsterdam) 6*, 891–899.
6. McDonald, J. P., Rapic-Otrin, V., Epstein, J. A., Broughton, B. C., Wang, X., Lehmann, A. R., Wolgemuth, D. J., and Woodgate, R. (1999) Novel human and mouse homologs of *Saccharomyces cerevisiae* DNA polymerase η. *Genomics 60*, 20–30.
7. Ohmori, H., Friedberg, E. C., Fuchs, R. P., Goodman, M. F., Hanaoka, F., Hinkle, D., Kunkel, T. A., Lawrence, C. W., Livneh, Z., Nohmi, T., Prakash, L., Prakash, S., Todo, T., Walker, G. C., Wang, Z., and Woodgate, R. (2001) The Y-family of DNA polymerases. *Mol. Cell 8*, 7–8.
8. Tissier, A., McDonald, J. P., Frank, E. G., and Woodgate, R. (2000) Polι, a remarkably error-prone human DNA polymerase. *Genes Dev. 14*, 1642–1650.
9. Vaisman, A., Lehmann, A. R., and Woodgate, R. (2004) DNA polymerases η and ι. *Adv. Protein Chem. 69*, 205–228.
10. Zhang, Y., Yuan, F., Wu, X., and Wang, Z. (2000) Preferential incorporation of G opposite template T by the low-fidelity human DNA polymerase ι. *Mol. Cell. Biol. 20*, 7099–7108.
11. McCulloch, S. D., and Kunkel, T. A. (2008) The fidelity of DNA synthesis by eukaryotic replicative and translesion synthesis polymerases. *Cell Res. 18*, 148–161.
12. Yang, W., and Woodgate, R. (2007) What a difference a decade makes: insights into translesion DNA synthesis. *Proc. Natl. Acad. Sci. U.S.A. 104*, 15591–15598.
13. Nair, D. T., Johnson, R. E., Prakash, S., Prakash, L., and Aggarwal, A. K. (2004) Replication by human DNA polymerase ι occurs by Hoogsteen base-pairing. *Nature 430*, 377–380.
14. Nair, D. T., Johnson, R. E., Prakash, L., Prakash, S., and Aggarwal, A. K. (2005) Human DNA polymerase ι incorporates dCTP opposite template G via a G•C $^{+}$ Hoogsteen base pair. *Structure 13*, 1569–1577.
15. Nair, D. T., Johnson, R. E., Prakash, L., Prakash, S., and Aggarwal, A. K. (2006) An incoming nucleotide imposes an *anti* to *syn* conformational change on the templating purine in the human DNA polymerase ι active site. *Structure 14*, 749–755.
16. Ling, H., Boudsocq, F., Woodgate, R., and Yang, W. (2001) Crystal structure of a Y-family DNA polymerase in action: a mechanism for error-prone and lesion-bypass replication. *Cell 107*, 91–102.
17. Lone, S., Townson, S. A., Uljon, S. N., Johnson, R. E., Brahma, A., Nair, D. T., Prakash, S., Prakash, L., and Aggarwal, A. K. (2007) Human DNA polymerase κ encircles DNA: implications for mismatch extension and lesion bypass. *Mol. Cell 25*, 601–614.
18. Alt, A., Lammens, K., Chiocchini, C., Lammens, A., Pieck, J. C., Kuch, D., Hopfner, K. P., and Carell, T. (2007) Bypass of DNA lesions generated during anticancer treatment with cisplatin by DNA polymerase η. *Science 318*, 967–970.
19. Nair, D. T., Johnson, R. E., Prakash, L., Prakash, S., and Aggarwal, A. K. (2006) Hoogsteen base pair formation promotes synthesis opposite the 1,N^6-ethenodeoxyadenosine lesion by human DNA polymerase ι. *Nat. Struct. Mol. Biol. 13*, 619–625.
20. Rechkoblit, O., Zhang, Y., Guo, D., Wang, Z., Amin, S., Krzeminsky, J., Louneva, N., and Geacintov, N. E. (2002) Trans-lesion synthesis past bulky benzo[*a*]pyrene diol epoxide N^2-dG and N^6-dA lesions catalyzed by DNA bypass polymerases. *J. Biol. Chem. 277*, 30488–30494.
21. Washington, M. T., Minko, I. G., Johnson, R. E., Wolfle, W. T., Harris, T. M., Lloyd, R. S., Prakash, S., and Prakash, L. (2004) Efficient and error-free replication past a minor-groove DNA adduct by the sequential action of human DNA polymerases ι and κ. *Mol. Cell. Biol. 24*, 5687–5693.
22. Wolfle, W. T., Johnson, R. E., Minko, I. G., Lloyd, R. S., Prakash, S., and Prakash, L. (2005) Human DNA polymerase ι promotes replication through a ring-closed minor-groove adduct that adopts a *syn* conformation in DNA. *Mol. Cell. Biol. 25*, 8748–8754.
23. Johnson, R. E., Yu, S. L., Prakash, S., and Prakash, L. (2007) A role for yeast and human translesion synthesis DNA polymerases in promoting replication through 3-methyl adenine. *Mol. Cell. Biol. 27*, 7198–7205.

24. Plosky, B. S., Frank, E. G., Berry, D. A., Vennall, G. P., McDonald, J. P., and Woodgate, R. (2008) Eukaryotic Y-family polymerases bypass a 3-methyl-2′-deoxyadenosine analog *in vitro* and methyl methanesulfonate-induced DNA damage *in vivo*. *Nucleic Acids Res. 36*, 2152–2162.
25. Choi, J. Y., and Guengerich, F. P. (2006) Kinetic evidence for inefficient and error-prone bypass across bulky N^2-guanine DNA adducts by human DNA polymerase ι. *J. Biol. Chem. 281*, 12315–12324.
26. Johnson, R. E., Prakash, L., and Prakash, S. (2005) Biochemical evidence for the requirement of Hoogsteen base pairing for replication by human DNA polymerase ι. *Proc. Natl. Acad. Sci. U.S.A. 102*, 10466–10471.
27. Johnson, R. E., Haracska, L., Prakash, L., and Prakash, S. (2006) Role of Hoogsteen edge hydrogen bonding at template purines in nucleotide incorporation by human DNA polymerase ι. *Mol. Cell. Biol. 26*, 6435–6441.
28. Potapova, O., Chan, C., DeLucia, A. M., Helquist, S. A., Kool, E. T., Grindley, N. D., and Joyce, C. M. (2006) DNA polymerase catalysis in the absence of Watson-Crick hydrogen bonds: analysis by single-turnover kinetics. *Biochemistry 45*, 890–898.
29. Mizukami, S., Kim, T. W., Helquist, S. A., and Kool, E. T. (2006) Varying DNA base-pair size in subangstrom increments: evidence for a loose, not large, active site in low-fidelity Dpo4 polymerase. *Biochemistry 45*, 2772–2778.
30. Johnson, R. E., Washington, M. T., Haracska, L., Prakash, S., and Prakash, L. (2000) Eukaryotic polymerases ι and ζ act sequentially to bypass DNA lesions. *Nature 406*, 1015–1019.
31. Wilson, R. H., DeEds, F., and Cox, A. J. (1941) The toxicity and carcinogenicity of 2-acetylaminofluorene. *Cancer Res. 1*, 595–608.
32. Heflich, R. H., and Neft, R. E. (1994) Genetic toxicity of 2-acetylaminofluorene, 2-aminofluorene and some of their metabolites and model metabolites. *Mutat. Res. 318*, 73–114.
33. Kriek, E. (1992) Fifty years of research on *N*-acetyl-2-aminofluorene, one of the most versatile compounds in experimental cancer research. *J. Cancer Res. Clin. Oncol. 118*, 481–489.
34. Suzuki, N., Ohashi, E., Hayashi, K., Ohmori, H., Grollman, A. P., and Shibutani, S. (2001) Translesional synthesis past acetylaminofluorene-derived DNA adducts catalyzed by human DNA polymerase κ and *Escherichia coli* DNA polymerase IV. *Biochemistry 40*, 15176–15183.
35. Doisy, R., and Tang, M. S. (1995) Effect of aminofluorene and (acetylamino)fluorene adducts on the DNA replication mediated by *Escherichia coli* polymerases I (Klenow fragment) and III. *Biochemistry 34*, 4358–4368.
36. Belguise-Valladier, P., Maki, H., Sekiguchi, M., and Fuchs, R. P. (1994) Effect of single DNA lesions on *in vitro* replication with DNA polymerase III holoenzyme. Comparison with other polymerases. *J. Mol. Biol. 236*, 151–164.
37. Shibutani, S., Suzuki, N., and Grollman, A. P. (1998) Mutagenic specificity of (acetylamino)fluorene-derived DNA adducts in mammalian cells. *Biochemistry 37*, 12034–12041.
38. Gillet, L. C., Alzeer, J., and Scharer, O. D. (2005) Site-specific incorporation of *N*-(deoxyguanosin-8-yl)-2-acetylaminofluorene (dG-AAF) into oligonucleotides using modified "ultra-mild" DNA synthesis. *Nucleic Acids Res. 33*, 1961–1969.
39. Gunz, D., Hess, M. T., and Naegeli, H. (1996) Recognition of DNA adducts by human nucleotide excision repair. Evidence for a thermodynamic probing mechanism. *J. Biol. Chem. 271*, 25089–25098.
40. Shibutani, S., Suzuki, N., Tan, X., Johnson, F., and Grollman, A. P. (2001) Influence of flanking sequence context on the mutagenicity of acetylaminofluorene-derived DNA adducts in mammalian cells. *Biochemistry 40*, 3717–3722.
41. Fuchs, R. P., and Fujii, S. (2007) Translesion synthesis in *Escherichia coli*: lessons from the *Nar*I mutation hot spot. *DNA Repair (Amsterdam) 6*, 1032–1041.
42. Fuchs, R. P., Koffel-Schwartz, N., Pelet, S., Janel-Bintz, R., Napolitano, R., Becherel, O. J., Broschard, T. H., Burnouf, D. Y., and Wagner, J. (2001) DNA polymerases II and V mediate respectively mutagenic (−2 frameshift) and error-free bypass of a single N^2-acetylaminofluorene adduct. *Biochem. Soc. Trans. 29*, 191–195.
43. Tan, X., Suzuki, N., Grollman, A. P., and Shibutani, S. (2002) Mutagenic events in *Escherichia coli* and mammalian cells generated in response to acetylaminofluorene-derived DNA adducts positioned in the *NarI* restriction enzyme site. *Biochemistry 41*, 14255–14262.
44. O'Handley, S. F., Sanford, D. G., Xu, R., Lester, C. C., Hingerty, B. E., Broyde, S., and Krugh, T. R. (1993) Structural characterization of an *N*-acetyl-2-aminofluorene (AAF) modified DNA oligomer by NMR, energy minimization, and molecular dynamics. *Biochemistry 32*, 2481–2497.
45. Patel, D. J., Mao, B., Gu, Z., Hingerty, B. E., Gorin, A., Basu, A. K., and Broyde, S. (1998) Nuclear magnetic resonance solution structures of covalent aromatic amine-DNA adducts and their mutagenic relevance. *Chem. Res. Toxicol. 11*, 391–407.
46. Cho, B. P., and Zhou, L. (1999) Probing the conformational heterogeneity of the acetylaminofluorene-modified 2′-deoxyguanosine and DNA by ^{19}F NMR spectroscopy. *Biochemistry 38*, 7572–7583.
47. Cho, B. P. (2004) Dynamic conformational heterogeneities of carcinogen-DNA adducts and their mutagenic relevance. *J. Environ. Sci. Health 22*, 57–90.
48. Evans, F. E., Miller, D. W., and Levine, R. A. (1986) ^{1}H NMR study of self-association and restricted internal rotation of the C8-substituted deoxyguanosine 5′-monophosphate adduct of the carcinogen 2-(acetylamino)fluorene. *J. Biomol. Struct. Dyn. 3*, 935–948.
49. Zhang, Y., Yuan, F., Wu, X., Taylor, J. S., and Wang, Z. (2001) Response of human DNA polymerase ι to DNA lesions. *Nucleic Acids Res. 29*, 928–935.
50. Grunberger, D., Nelson, J. H., Cantor, C. R., and Weinstein, I. B. (1970) Coding and conformational properties of oligonucleotides modified with the carcinogen N^2-acetylaminofluorene. *Proc. Natl. Acad. Sci. U.S.A. 66*, 488–494.
51. Fuchs, R., and Daune, M. (1972) Physical studies on deoxyribonucleic acid after covalent binding of a carcinogen. *Biochemistry 11*, 2659–2666.
52. Fuchs, R., and Daune, M. (1971) Changes of stability and conformation of DNA following the covalent binding of a carcinogen. *FEBS Lett. 14*, 206–208.
53. Milhe, C., Dhalluin, C., Fuchs, R. P., and Lefevre, J. F. (1994) NMR evidence of the stabilisation by the carcinogen N^2-acetylaminofluorene of a frameshift mutagenesis intermediate. *Nucleic Acids Res. 22*, 4646–4652.
54. Wang, L., and Broyde, S. (2006) A new *anti* conformation for *N*-(deoxyguanosin-8-yl)-2-acetylaminofluorene (AAF-dG) allows Watson-Crick pairing in the *Sulfolobus solfataricus* P2 DNA polymerase IV (Dpo4). *Nucleic Acids Res. 34*, 785–795.
55. Berman, H. M., Westbrook, J., Feng, Z., Gilliland, G., Bhat, T. N., Weissig, H., Shindyalov, I. N., and Bourne, P. E. (2000) The Protein Data Bank. *Nucleic Acids Res. 28*, 235–242.
56. Fiser, A., Do, R. K., and Sali, A. (2000) Modeling of loops in protein structures. *Protein Sci. 9*, 1753–1773.
57. Fiser, A., and Sali, A. (2003) ModLoop: automated modeling of loops in protein structures. *Bioinformatics 19*, 2500–2501.
58. van Meerssche, M., Germain, G., Declercq, J.-P., Touillaux, R., Roberfroid, M., and Razzouk, C. (1980) 2-(Acetylamino)fluorene, C15H13NO. *Acta Crystallogr., Sect. C: Cryst. Struct. Commun 9*, 515–518.
59. Allen, F. H. (2002) The Cambridge Structural Database: a quarter of a million crystal structures and rising. *Acta Crystallogr. 58*, 380–388.
60. Cornell, W. D., Cieplak, P., Bayly, C. I., Gould, I. R., Merz, K. M., Ferguson, D. M., Spellmeyer, D. C., Fox, T., Caldwell, J. W., and Kollman, P. A. (1995) A second generation force field for the simulation of proteins, nucleic acids, and organic molecules. *J. Am. Chem. Soc. 117*, 5179–5197.
61. Duan, Y., Wu, C., Chowdhury, S., Lee, M. C., Xiong, G., Zhang, W., Yang, R., Cieplak, P., Luo, R., Lee, T., Caldwell, J., Wang, J., and Kollman, P. (2003) A point-charge force field for molecular mechanics simulations of proteins based on condensed-phase quantum mechanical calculations. *J. Comput. Chem. 24*, 1999–2012.
62. Cheatham, T. E., III., Cieplak, P., and Kollman, P. A. (1999) A modified version of the Cornell et al. force field with improved sugar pucker phases and helical repeat. *J. Biomol. Struct. Dyn. 16*, 845–862.
63. Wang, J. M., Cieplak, P., and Kollman, P. A. (2000) How well does a restrained electrostatic potential (RESP) model perform in calculating conformational energies of organic and biological molecules? *J. Comput. Chem. 21*, 1049–1074.
64. Hehre, W. J., Ditchfie, R., and Pople, J. A. (1972) Self-consistent molecular-orbital methods. 12. Further extensions of Gaussian-type basis sets for use in molecular-orbital studies of organic-molecules. *J. Chem. Phys. 56*, 2257–2261.
65. Frisch, M. J., Schlegel, H. B., Scuseria, G. E., Robb, M. A., Cheeseman, J. R., Montgomery, J., J. A., Vreven, T., Kudin, K. N., Burant, J. C., Millam, J. M., Iyengar, S. S., Tomasi, J., Barone, V.,

Mennucci, B., Cossi, M., Scalmani, G., Rega, N., Petersson, G. A., Nakatsuji, H., Hada, M., Ehara, M., Toyota, K., Fukuda, R., Hasegawa, J., Ishida, M., Nakajima, T., Honda, Y., Kitao, O., Nakai, H., Klene, M., Li, X., Knox, J. E., Hratchian, H. P., Cross, J. B., Bakken, V., Adamo, C., Jaramillo, J., Gomperts, R., Stratmann, R. E., Yazyev, O., Austin, A. J., Cammi, R., Pomelli, C., Ochterski, J. W., Ayala, P. Y., Morokuma, K., Voth, G. A., Salvador, P., Dannenberg, J. J., Zakrzewski, V. G., Dapprich, S., Daniels, A. D., Strain, M. C., Farkas, O., Malick, D. K., Rabuck, A. D., Raghavachari, K., Foresman, J. B., Ortiz, J. V., Cui, Q., Baboul, A. G., Clifford, S., Cioslowski, J., Stefanov, B. B., Liu, G., Liashenko, A., Piskorz, P., Komaromi, I., Martin, R. L., Fox, D. J., Keith, T., Al-Laham, M. A., Peng, C. Y., Nanayakkara, A., Challacombe, M., Gill, P. M. W., Johnson, B., Chen, W., Wong, M. W., Gonzalez, C., and Pople, J. A. (2004) Gaussian 03, Gaussian, Inc., Wallingford, CT.

66. Bayly, C. I., Cieplak, P., Cornell, W. D., and Kollman, P. A. (1993) A well-behaved electrostatic potential based method using charge restraints for deriving atomic charges—the RESP model. *J. Phys. Chem. 97*, 10269–10280.
67. Cieplak, P., Cornell, W. D., Bayly, C., and Kollman, P. A. (1995) Application of the multimolecule and multiconformational RESP methodology to biopolymers-charge derivation for DNA, RNA, and proteins. *J. Chem. Phys. 16*, 1357–1377.
68. Perlow, R. A., and Broyde, S. (2002) Toward understanding the mutagenicity of an environmental carcinogen: structural insights into nucleotide incorporation preferences. *J. Mol. Biol. 322*, 291–309.
69. Wang, J., Wolf, R. M., Caldwell, J. W., Kollman, P. A., and Case, D. A. (2004) Development and testing of a general amber force field. *J. Comput. Chem. 25*, 1157–1174.
70. Case, D. A., Darden, T. A., Cheatham, T. E., III., Simmerling, C. L., Wang, J., Duke, R. E., Luo, R., Merz, K. M., Wang, B., Pearlman, D. A., Crowley, M., Brozell, S., Tsui, V., Gohlke, H., Mongan, J., Hornak, V., Cui, G., Beroza, P., Schafmeister, C., Caldwell, J. W., Ross, W. S., and Kollman, P. A. (2004) AMBER 8, University of California, San Francisco.
71. Mezei, M. (1997) Optimal position of the solute for simulations. *J. Comput. Chem. 18*, 812–815.
72. Jorgensen, W. L., Chandrasekhar, J., Madura, J. D., Impey, R. W., and Klein, M. L. (1983) Comparison of simple potential functions for simulating liquid water. *J. Chem. Phys. 79*, 926–935.
73. Darden, T., York, D., and Pedersen, L. (1993) Particle mesh Ewald—an nlog (n) method for Ewald sums in large systems. *J. Chem. Phys. 98*, 10089–10092.
74. Essmann, U., Perera, L., Berkowitz, M. L., Darden, T., Lee, H., and Pedersen, L. G. (1995) A smooth particle mesh Ewald method. *J. Chem. Phys. 103*, 8577–8593.
75. Ryckaert, J. P., Ciccotti, G., and Berendsen, H. J. C. (1977) Numerical-integration of Cartesian equations of motion of a system with constraints-molecular-dynamics of *N*-alkanes. *J. Comput. Phys. 23*, 327–341.
76. Berendsen, H. J. C., Postma, J. P. M., van Gunsteren, W. F., DiNola, A., and Haak, J. R. (1984) Molecular dynamics with coupling to an external bath. *J. Chem. Phys. 81*, 3684–3690.
77. Harvey, S. C., Tan, R. K. Z., and Cheatham, T. E. (1998) The flying ice cube: Velocity rescaling in molecular dynamics leads to violation of energy equipartition. *J. Comput. Chem. 19*, 726–740.
78. Simmerling, C., Elber, R., and Zhang, J. (1995) MOIL-View—A program for visualization of structure and dynamics of biomolecules and STO-A program for computing stochastic paths, in *Modeling of Biomolecular Structure and Mechanisms* (Pullman, A., et al., Eds.) pp 241−265, Kluwer, The Netherlands.
79. Batra, V. K., Beard, W. A., Shock, D. D., Krahn, J. M., Pedersen, L. C., and Wilson, S. H. (2006) Magnesium-induced assembly of a complete DNA polymerase catalytic complex. *Structure 14*, 757–766.
80. Wang, L., Yu, X., Hu, P., Broyde, S., and Zhang, Y. (2007) A water-mediated and substrate-assisted catalytic mechanism for *Sulfolobus solfataricus* DNA polymerase IV. *J. Am. Chem. Soc. 129*, 4731–4737.
81. Shankar, K., Djamal, B., Robert, H. S., Peter, A. K., and John, M. R. (1992) The weighted histogram analysis method for free-energy calculations on biomolecules. I: The method. *J. Comput. Chem. 13*, 1011–1021.
82. Saenger, W. (1984) *Principles of Nucleic Acid Structure*, Springer-Verlag, New York.
83. Plum, G. E., and Breslauer, K. J. (1995) Thermodynamics of an intramolecular DNA triple helix: a calorimetric and spectroscopic study of the pH and salt dependence of thermally induced structural transitions. *J. Mol. Biol. 248*, 679–695.
84. Asensio, J. L., Lane, A. N., Dhesi, J., Bergqvist, S., and Brown, T. (1998) The contribution of cytosine protonation to the stability of parallel DNA triple helices. *J. Mol. Biol. 275*, 811–822.
85. Wu, P., Kawamoto, Y., Hara, H., and Sugimoto, N. (2002) Effect of divalent cations and cytosine protonation on thermodynamic properties of intramolecular DNA double and triple helices. *J. Inorg. Biochem. 91*, 277–285.
86. Zimmer, C., Luck, G., Venner, H., and Fric, J. (1968) Studies on the conformation of protonated DNA. *Biopolymers 6*, 563–574.
87. Frank, E. G., and Woodgate, R. (2007) Increased catalytic activity and altered fidelity of human DNA polymerase ι in the presence of manganese. *J. Biol. Chem. 282*, 24689–24696.
88. Oelschlaeger, P., Klahn, M., Beard, W. A., Wilson, S. H., and Warshel, A. (2007) Magnesium-cationic dummy atom molecules enhance representation of DNA polymerase beta in molecular dynamics simulations: improved accuracy in studies of structural features and mutational effects. *J. Mol. Biol. 366*, 687–701.
89. Adcock, S. A., and McCammon, J. A. (2006) Molecular dynamics: survey of methods for simulating the activity of proteins. *Chem. Rev. 106*, 1589–1615.
90. Frank, E. G., Sayer, J. M., Kroth, H., Ohashi, E., Ohmori, H., Jerina, D. M., and Woodgate, R. (2002) Translesion replication of benzo[*a*]pyrene and benzo[*c*]phenanthrene diol epoxide adducts of deoxyadenosine and deoxyguanosine by human DNA polymerase ι. *Nucleic Acids Res. 30*, 5284–5292.
91. Tissier, A., Frank, E. G., McDonald, J. P., Iwai, S., Hanaoka, F., and Woodgate, R. (2000) Misinsertion and bypass of thymine-thymine dimers by human DNA polymerase ι. *EMBO J. 19*, 5259–5266.
92. Vaisman, A., Takasawa, K., Iwai, S., and Woodgate, R. (2006) DNA polymerase ι-dependent translesion replication of uracil containing cyclobutane pyrimidine dimers. *DNA Repair (Amsterdam) 5*, 210–218.
93. Vaisman, A., Frank, E. G., McDonald, J. P., Tissier, A., and Woodgate, R. (2002) Polι-dependent lesion bypass *in vitro*. *Mutat. Res. 510*, 9–22.
94. Wang, Y., Woodgate, R., McManus, T. P., Mead, S., McCormick, J. J., and Maher, V. M. (2007) Evidence that in xeroderma pigmentosum variant cells, which lack DNA polymerase η, DNA polymerase ι causes the very high frequency and unique spectrum of UV-induced mutations. *Cancer Res. 67*, 3018–3026.

BI801283D